Magnetic Studies of the Canted Ising Linear Chain $CsCoCl_3 \cdot 2H_2O$

A. Herweijer, W.J.M. de Jonge, A.C. Botterman,* A.L.M. Bongaarts, and J. A. Cowen†
Department of Physics, Eindhoven University of Technology, Eindhoven, The Netherlands
(Received 26 October 1971)

Specific-heat, nuclear-magnetic-resonance, magnetic-susceptibility, magnetization, and antiferromagnetic-resonance measurements on the orthorhombic crystal $CsCoCl_3 \cdot 2H_2O$ have led to the following model of the magnetic structure and the exchange interactions: The interaction is Ising-like with very strong exchange along the $\vec{a}$ axis resulting in canted-antiferromagnetic chains lying in the *ac* plane with their moments 10° from the $\vec{c}$ axis and a net moment in the $\vec{a}$ direction. At $T_N = 3.38$ K the chains in each *ac* plane couple ferromagnetically so that their net moments are all in the same sense, but with the net moments in alternate planes antiparallel. At a critical field of 2.9 kOe at 1.1 K ($\vec{H}$ applied along the $\vec{a}$ axis) the moments in half of the planes reverse giving rise to an induced ferromagnetic moment parallel to the $\vec{a}$ axis. At temperatures well above T_N the strong Ising interaction produces correlations which manifest themselves as a large induced moment at relatively modest fields. The general features of these experimental results have been reproduced using a Hamiltonian which includes Ising and Dzyaloshinsky-Moriya terms for the interaction along the $\vec{a}$ axis and isotropic terms for the interactions along $\vec{b}$ and $\vec{c}$. Applying this Hamiltonian to the critical-field and antiferromagnetic-resonance data, we obtain the following values: $J^a = -13$ K, $J^b = -0.2$ K, $J^c = +4.5$ K, and $D = +3.6$ K. These numerical values are the result of applying a very simplified model to a very complex system and thus must be considered as qualitative rather than quantitative.

I. INTRODUCTION

A classical technique in the field of magnetism involves the study of isostructural salts which have either the same magnetic ion and different ligands or different magnetic ions and the same ligands. $CsMnCl_3 \cdot 2H_2O$ has become a standard example of a one-dimensional Heisenberg antiferromagnet.[1,2] The replacement of Mn^{2+} by Co^{2+} results in the isostructural salt $CsCoCl_3 \cdot 2H_2O$ which, since Co^{2+} often appears Ising-like,[3] is likely to be an example of an Ising linear chain.

We have measured the specific heat, nuclear-magnetic resonance (NMR), magnetization, dynamic susceptibility, and antiferromagnetic resonance (AFMR) of $CsCoCl_3 \cdot {}_2H_2O$. From these measurements we have deduced a magnetic structure and evaluated the exchange parameters.

The measurements and interpretation are presented in a sequence which purports to give a logical development of our ideas. Needless to say, this was not the sequence in which the ideas occurred. Nonetheless, it makes a pedagogically interesting and logical picture. Thus, Sec. II describes the crystallography and preparation, while Secs. III–VI give the results of specific-heat, NMR, magnetization and susceptibility, and AFMR measurements, along with their interpretation.

In Secs. VII and IX, we derive a detailed model of the exchange interactions and summarize our conclusions with a table which indicates not only the final model but also the contribution of each individual experiment in arriving at the conclusions.

A brief report of some of these results has appeared previously.[4]

II. STRUCTURE AND PREPARATION

The structure of $CsCoCl_3 \cdot 2H_2O$, as determined by Thorup and Soling,[5] was shown to be identical to that of $CsMnCl_3 \cdot 2H_2O$. The room-temperature crystallographic space group is *Pcca* and the chemical unit cell contains four formula units. The atomic parameters and lattice constants are summarized in Table I. The structure consists of octahedra of four chlorine and two oxygen atoms. The Cl_I-Co-Cl_I axis of each octahedron lies very near to the *ac* plane and makes an angle of 64° with the crystallographic $\vec{c}$ axis. The octahedra share one chlorine, thus forming chains along the $\vec{a}$ axis (Fig. 1). Alternate octahedra along the $\vec{a}$ axis make angles of ±64°. The chains are separated in the $\vec{b}$ direction by layers of cesium atoms and in the $\vec{c}$ direction by layers of hydrogen atoms which probably cause the easy cleavage parallel to the *ab* plane.

Single crystals used in all of the experiments were grown by evaporation at room temperature from a solution of $CoCl_2 \cdot 6H_2O$ and CsCl in a molar ratio of 4.8 : 1. The characteristic deep-blue crystals were platelike and not very well developed in the $\vec{c}$ direction.

III. SPECIFIC HEAT

Specific-heat measurements were performed on a sample consisting of approximately 26 g of small crystals (average linear dimension 0.5 mm), using a standard exchange-gas–type ^{4}He calorimeter. The

TABLE I. Room-temperature atomic coordinates of $CsCoCl_3 \cdot 2H_2O$ (data from Ref. 5).

Atoms	$a = 8.914$ Å X	$b = 7.174$ Å Y	$c = 11.360$ Å Z
Cs	0.2500	0.0000	0.1455
Co	0.0000	0.4727	0.2500
Cl_I	0.2500	0.5000	0.1529
Cl_{II}	0.0866	0.2344	0.3879
O	0.0659	0.6795	0.3661

sample was sealed in a copper capsule together with a small amount (10 Torr at 77 K) of ^{4}He exchange gas. Care was taken to prevent the crystals from dehydrating during the backfill process by precooling to liquid-nitrogen temperature. The sample holder carried a noninductively wound heater and a calibrated germanium thermometer.[6]

The interpolation of the calibration data was based on two separate 8 deg polynomials. The standard deviations of the fits for 29 data points in the temperature range 1.5–12 K and 36 points in the range 9–100 K were 0.05% and 0.01%, respectively. The heat capacity of the empty capsule was determined in a separate experimental run.

The experimental data in the range 1.5–30 K are shown in Fig. 2. The specific heat of $CsCoCl_3 \cdot 2H_2O$ is seen to pass through a sharp—but relatively small—anomaly at 3.38 K which accompanies the cooperative ordering of the Co spins at that temperature. The small anomaly occurring at 2.3 K is due to the magnetic transition of about 0.2 g of $CoCl_2 \cdot 6H_2O$, an impurity which we were unable to avoid in the crystal-growing process.

In order to evaluate the magnetic contribution to the total specific heat we must subtract the contribution of the lattice specific heat. This turned

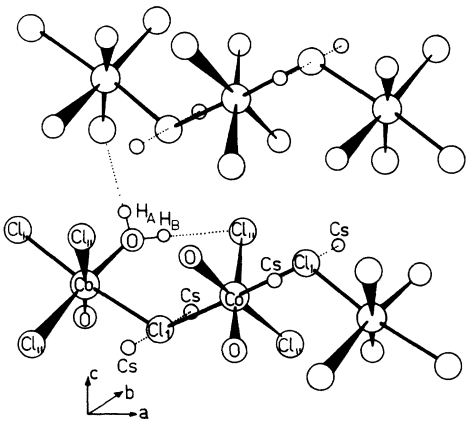

FIG. 1. Structure of $CsCoCl_3 \cdot 2H_2O$ according to Thorup and Soling (Ref. 5). Only one set of hydrogen atoms and hydrogen bonds are shown.

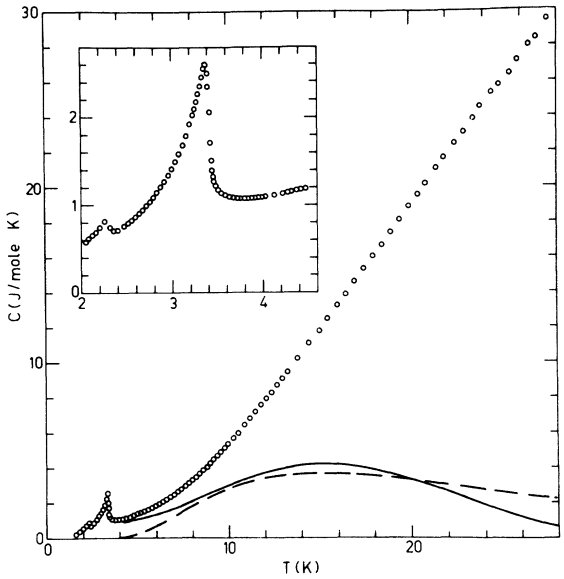

FIG. 2. Specific heat from 1 to 30 K. The circles are the measured values. The solid line is the magnetic part after subtraction of a typical lattice term. Dashed curve is an Ising calculation with $J = 72$ K.

out to be a difficult problem. In an attempt to separate the two contributions, a plot of $C_p T^2$ vs T^5 was made for the range 6–10 K. The plot showed serious deviations from a straight line. If we assume that in this region the lattice term can be approximated by a T^3 law, this suggests that the magnetic term cannot be described by a T^{-2} law as in the case of an isotropic Heisenberg system.

Attempts to grow a diamagnetic isomorphic crystal, in order to obtain a quantitative expression for the lattice contribution, were unsuccessful.

The total entropy gain below 4 K (including the lattice entropy and an estimated extrapolation below 1.5 K) amounts to only 16% of the theoretical value, $0.693R$, predicted for the ordering of a mole of Co spins with an effective spin $\frac{1}{2}$. This suggests the presence of an additional contribution to the magnetic specific heat due to a possible ordering of lower dimensionality above 4 K. The existence of such a term is further indicated by the peculiar linear behavior of the total specific heat in that range.

Numerical fits of the data to various expressions containing Debye functions for the lattice contribution and the theoretical formula for the one-dimensional Ising case[7]—despite the obviously arbitrary way in which the lattice is thus represented—all result in a rather high intrachain exchange parameter ($J^a > 40$ K). This result is not surprising if we compare the total experimental specific heat with the theoretical maximum of the one-dimensional Ising case ($C_{p\,\max} = 3.6$ J/mole K).

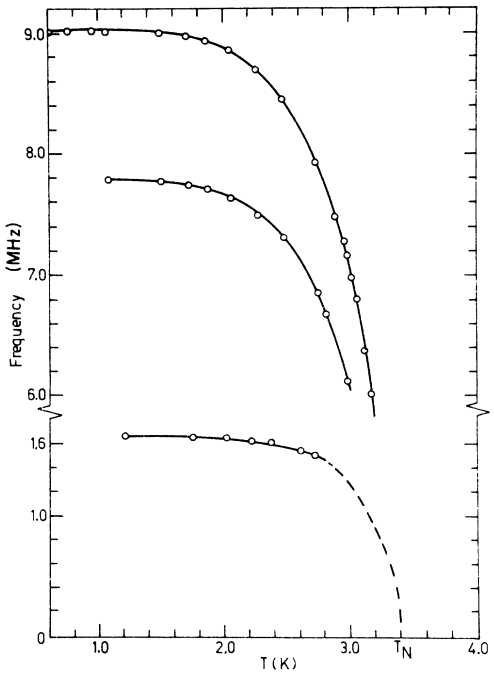

FIG. 3. Temperature dependence of the proton (upper two curves) and Cs (lower curve) nuclear-magnetic-resonance frequency.

IV. NUCLEAR MAGNETIC RESONANCE

A. Experimental Results

In zero external magnetic field and below 3.38 K we observed two proton resonances, seven cesium resonances, and three very weak chlorine resonances. The temperature dependence of the proton and cesium lines is shown in Fig. 3. We observed two ^{35}Cl pure quadrupole resonances at 8.03 and 5.62 MHz, respectively. Above 3.38 K the width of the pure-quadrupole lines was quite normal (about 30 kHz) and indicated purely paramagnetic behavior. The temperature dependence of the chlorine resonances below 3.38 K is not shown because there are insufficient data to permit an interpretation. However, the fact that some of the Cl resonances were observed at frequencies below the pure quadrupole-resonance frequency suggests very strongly that the magnetic ordering in the chains is antiferromagnetic, as it is in $CsMnCl_3 \cdot 2H_2O$.

We determined the direction of the internal local fields at the proton and cesium sites by observing the splitting of the lines in a small applied external field. The results of these experiments are given in Table II. To each magnitude of the local field correspond eight symmetry-related local-field directions.

To determine the direction of the sublattice magnetization we attempted to construct the H-T phase diagram. Within the experimental limits of field and temperature available to us only one phase boundary could be found. The temperature dependence of this boundary is given in Fig. 4. The angle dependence of H_c vs θ can be described by $H_c = H_{c0}/\cos\theta$ and is plotted in Fig. 5.

The nature of the states on both sides of this boundary was investigated by performing rotation diagrams on the cesium resonance in the ac plane in a large—7.5 kOe—external field. From the angle dependence of the phase boundary (Fig. 5) it appears that in an external field of 7.5 kOe the system remains in the lower phase as long as H lies within 23° of the $\vec{c}$ axis. Rotating the field further from $\vec{c}$ brings the system into the higher state. The results of the rotation experiment are shown in Fig. 6 along with data taken at 4.2 K, i.e., above the transition temperature. Close to the $\vec{c}$ axis the cesium lines show a 360° periodicity, characteristic of the antiferromagnetic state, while for $\theta > 23°$ the periodicity is 180°, characteristic of the paramagnetic state. The data near the $\vec{c}$ axis agree perfectly with the dashed lines which are calculated by adding the known external field to the internal field obtained from the zero-field experiments at 1.2 K. The data in the upper phase agree very well with the data taken in the paramagnetic state at 4.2 K.

Similar experiments on the protons at 4.2 K also show the characteristic paramagnetic pattern. The shift in the proton resonance lines due to the susceptibility in the paramagnetic state becomes zero when the external field is applied along the $\vec{b}$ or $\vec{c}$

TABLE II. Local magnetic fields at various nuclear sites (Fig. 1). The values are calculated from a dipole sum using the space group $P_{2_1}cca'$ with the magnetic moments deviating 10° from $\vec{c}$ in the ac plane.

Site	Magn. (kOe) at 1.1 K.	Experimental Orientation[a] α β γ	Ratio H_A/H_B	Magn. (kOe) $\mu = 2.25\mu_B$	Calculation Orientation[a] α β γ	Ratio H_A/H_B
H_A	2.114	90° 62° 28°		2.106	90° 57° 33°	
H_B	1.797	35° 58° 77°	1.17	1.797	37° 56° 77°	1.17
Cs	3.000	90° 90° 0°		0.135	90° 90° 0°	

[a] With respect to $\vec{a}$, $\vec{b}$, and $\vec{c}$ axis.

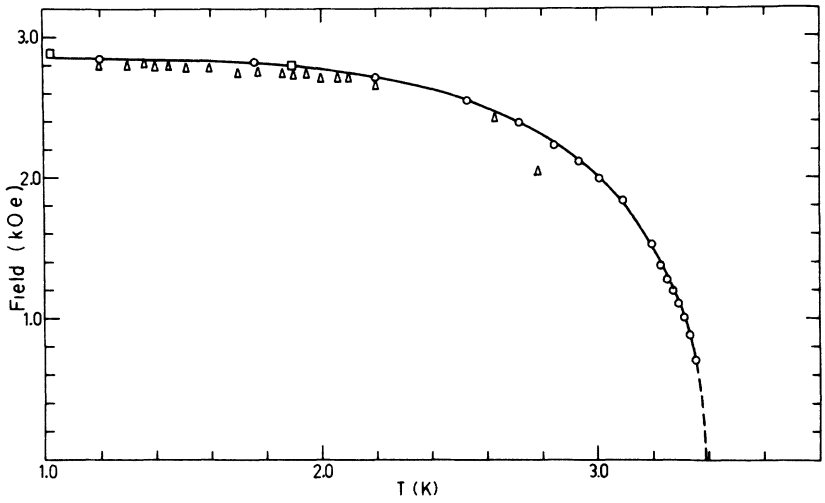

FIG. 4. Temperature dependence of the critical field. Circle—NMR, triangle—AFMR, square—magnetization.

axis indicating a large anisotropy in the g tensor.

B. Interpretation

The resonance data show that the symmetry of the local fields at the proton and cesium sites (the aspect group) can be described by *mmm*. There are a large number of invariant spin arrays (Shubnikov groups) which give rise to this local-field symmetry. However, if we define N_a as the number of elements in the aspect group, N_f as the number of distinct field magnitudes associated with one type of nucleus and N_n as the number of such nuclei per lattice point, then the ratio $N_a N_f / N_n$ gives us information about the nature of the magnetic space group.[8] In our case $N_a = 8$, $N_f = 2$, and $N_n = 16$, so that the ratio is 1. If we assume that the chemical space group is *Pcca*, the magnetic space group contains either an inversion and at least one antitranslation or neither inversion nor antitranslation.

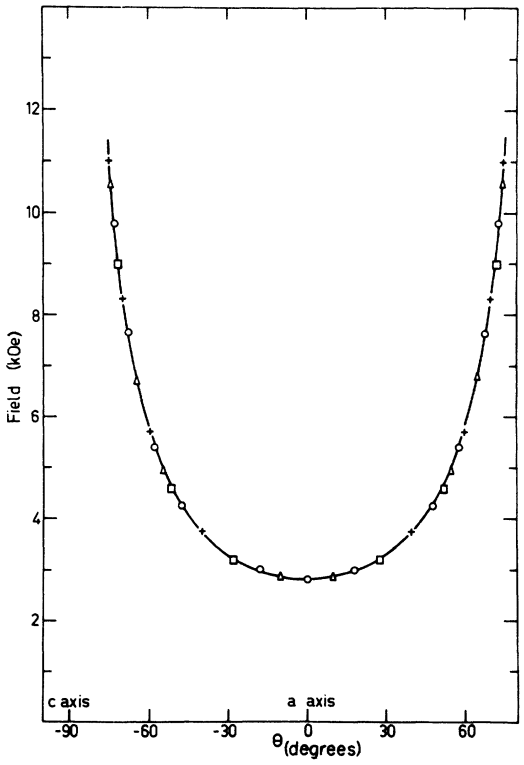

FIG. 5. Angle dependence of the critical field. Circle—NMR, triangle—AFMR, square—magnetization. Plus signs indicate the function $H_c = H_{c0}/\cos\theta$.

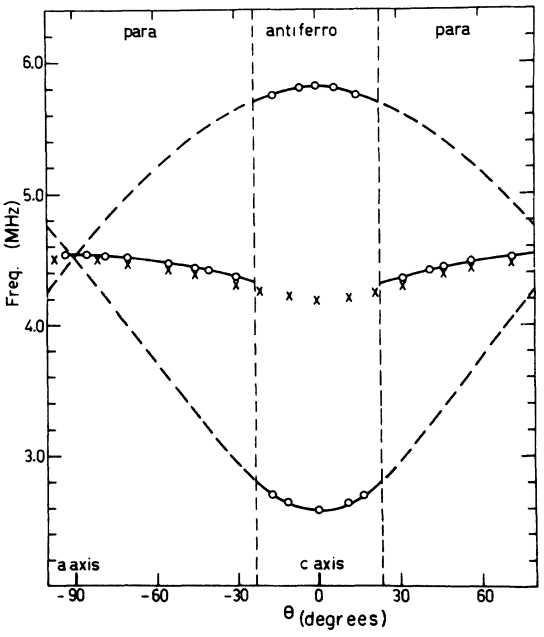

FIG. 6. Cs NMR frequency as a function of applied field direction at 7.5 kOe; circle—$T = 1.2$ K; X—$T = 4.2$ K. The dashed line is calculated using the known external field and the internal field obtained from zero-field experiments near 1.2 K.

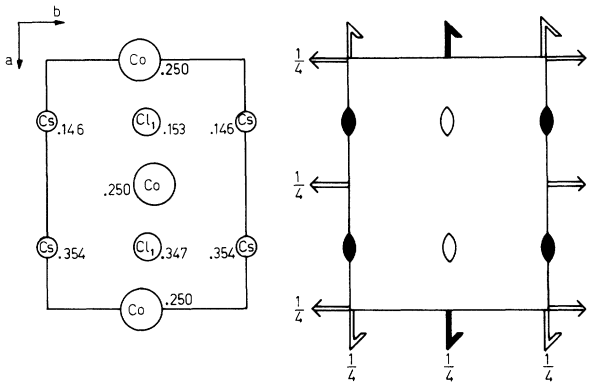

FIG. 7. Diagram at the left shows the position of the nuclei used to determine the nature of the twofold axes determined by the experiments. The figure at the right represents only one half the the magnetic unit cell. Standard crystallographic symbols for the axes have been used with the added convention that a black axis is an ordinary axis and a white axis is an antiaxis.

There are eight magnetic space groups belonging to the Opechowski[9] family of the crystallographic space group *Pcca* which satisfy this condition.

A further selection from among these eight is possible through the conditions set by the direction of the local field at the Cs site and the direction of the sublattice magnetization. The Co and Cs ions occupy special positions on the 2_y and 2_z axis, respectively (Fig. 7). Table II shows us that the local field at the Cs site is along the 2_z axis. This is only possible if the Cs ions lie on an uncolored twofold axis.

The direction of the sublattice magnetization may be restricted to either the $\vec{b}$ direction or the *ac* plane. Although none of the arguments is conclusive, the following points lead us to reject the first possibility: (i) The observed angle dependence of the phase boundary with a minimum in the $\vec{a}$ direction makes it unlikely that the magnetic moments are along $\vec{b}$. (ii) The large component of the internal field at the Cs site parallel to the $\vec{c}$ axis can only be explained by a significant contribution due to an isotropic hyperfine field along $\vec{c}$.

If the magnetization is in the *ac* plane, the 2_y axis through the Co site should transform to a colored axis in the magnetic state.

The magnetic space groups which satisfy these conditions are $P_{2b}c'ca$, $P_{2b}cca'$, and $Pcca'$. Symmetry does not require the Co moment to be directed along either the $\vec{a}$ or $\vec{c}$ axes so that we are still free to choose the sublattice magnetization anywhere in the *ac* plane.

A further aid in determining the direction of the sublattice magnetization is the dipole sum. Dipole calculations of the local fields at the proton sites for all of the above space groups reveal that the best agreement between the experimental and calculated values is obtained for the space group $P_{2b}cca'$ with the magnetic moments close to the $\vec{c}$ direction in the *ac* plane (Table II). Assuming $\mu = 2.25\mu_B$, the angle between the magnetic moments and the $\vec{c}$ axis $\phi = 10°$ gave excellent agreement with experiment. The resulting suggested sublattice array is shown in Fig. 8. The array may be described as a sheet of moments in the *ac* plane coupled almost antiferromagnetically along the $\vec{a}$ direction and coupled ferromagnetically along the $\vec{c}$ direction. The canting gives rise to a net magnetic moment in the $+\vec{a}$ direction. Moments in adjacent *ac* planes are coupled antiferromagnetically with the result that their net moments are in the $-\vec{a}$ direction.

The values for ϕ_m and μ quoted above should not be taken too seriously because the experimental fields must be compared with the sum of the dipolar and hyperfine fields at the proton sites. The latter contribution is generally small but not negligible. Assuming the proposed magnetic-moment structure to be correct, it will move the calculated field directions somewhat toward the positive $\vec{c}$ axis thus improving the agreement between the calculated and experimental fields.

V. MAGNETIZATION AND SUSCEPTIBILITY

A. Experimental Results

We have performed magnetization measurements with a Faraday balance at various temperatures between 1.1 and 300 K in fields up to 22 kOe. In order to obtain g values we have, in addition, measured the magnetization along the crystallographic axes at 1.5 K in fields up to 350 kOe. We have also

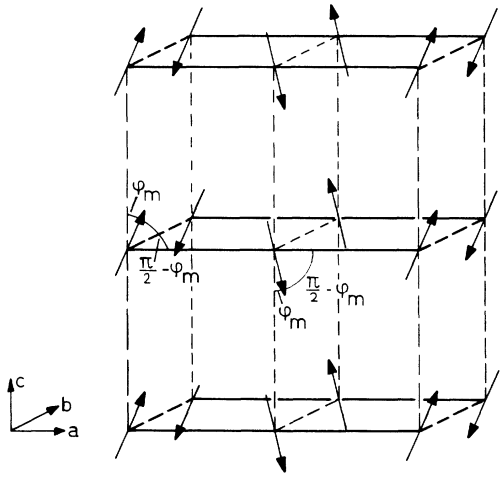

FIG. 8. Proposed magnetic-moment array. All spins lie in the *ac* plane. The model suggest ferromagnetic coupling along the $\vec{c}$ axis, antiferromagnetic coupling along the $\vec{b}$ axis, and essentially antiferromagnetic coupling along the $\vec{a}$ axis.

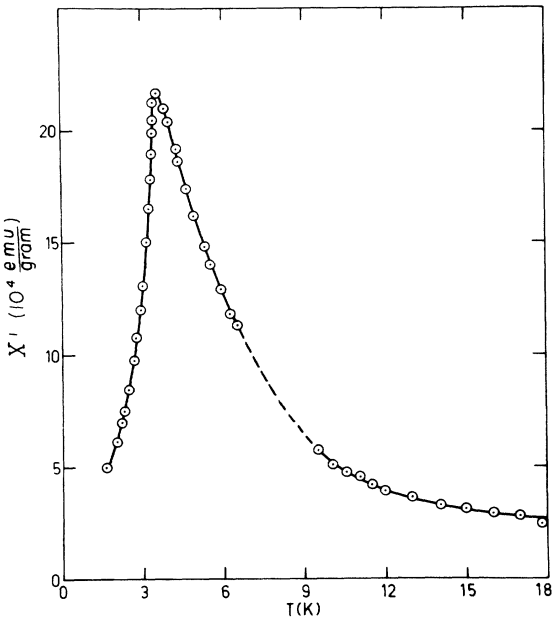

FIG. 9. Dynamic susceptibility of $CsCoCl_3 \cdot 2H_2O$ as a function of temperature with the alternating field parallel to the $\vec{a}$ axis.

measured the dynamic susceptibility between 1.1 and 20 K using a Wiebes inductance bridge[10] operating at 1200 Hz.

The real part of the dynamic susceptibility (χ') measured as a function of temperature along the $\vec{a}$ axis shows a large peak (Fig. 9). Defining the transition temperature as the point of maximum positive slope, we derive $T_N = 3.4$ K. Along the $\vec{b}$ and $\vec{c}$ axes χ' is essentially temperature independent. This is in agreement with the magnetization results. The magnetization measured along the $\vec{a}$ axis shows a maximum which shifts to lower temperature as the field is increased. Extrapolating the location of the maximum to zero field and assuming that this temperature is T_N, we find $T_N = 3.4 \pm 0.2$ K. Along the $\vec{b}$ and $\vec{c}$ axes, in the liquid-helium range the magnetization is essentially constant.

In order to determine the sublattice magnetization and hence the g values, we measured the magnetization in fields up to 350 kOe in the high-field magnet at the "Natuurkundig Laboratorium" of the University of Amsterdam. Even at 350 kOe $CsCoCl_3 \cdot 2H_2O$ is not completely saturated at 1.5 K, so that it was necessary to extrapolate the measurements to obtain the values given in Table III.

At high temperatures the susceptibility derived from the magnetization measurements exhibits Curie-Weiss behavior along the $\vec{b}$ axis (Fig. 10) but deviates from Curie-Weiss behavior along the $\vec{c}$ axis. Along the $\vec{a}$ axis the susceptibility is non-Curie-like for all temperatures covered by the measurements.

At temperatures well below T_N and in low fields the magnetization (σ) measured as a function of field shows the usual antiferromagnetic behavior (Fig. 11). At 1.1 K, for example, with H applied parallel to the $\vec{a}$ axis, the magnetization increases linearly up to a critical field field of 2900 Oe, exhibits a discontinuity of 10 emu/g at H_c, and continues to increase gradually with increasing field up to 350 kOe. If we extrapolate σ from, for example, 20 kOe back to zero field we observe an induced ferromagnetic moment σ_0. It is remarkable that this induced moment does not disappear as the temperature rises above T_N. Although the field range

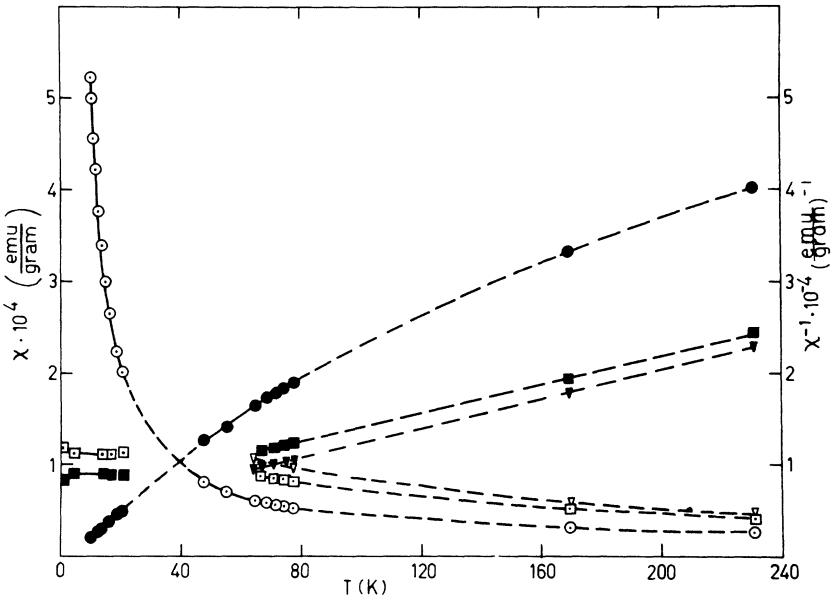

FIG. 10. Static susceptibility of $CsCoCl_3 \cdot 2H_2O$ (left scale and open symbols) and the inverse susceptibility (right scale and solid symbols) as a function of temperature; circles—$\vec{H} \parallel \vec{a}$; squares—$\vec{H} \parallel \vec{b}$, triangles—$\vec{H} \parallel \vec{c}$.

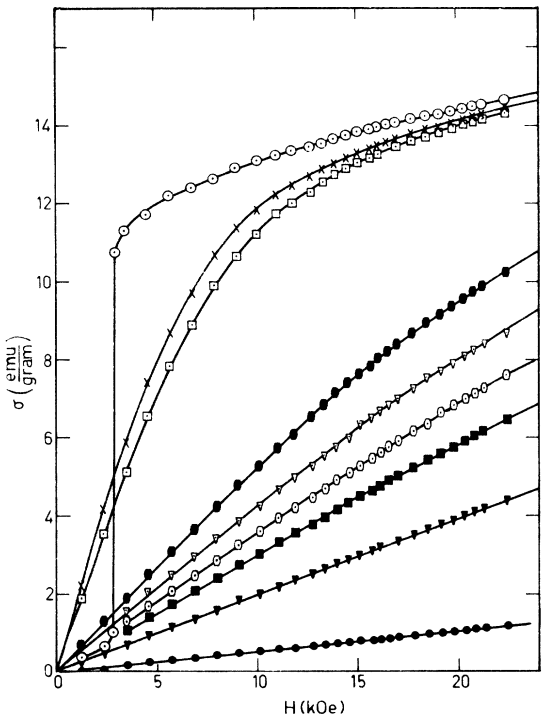

FIG. 11. Magnetization of $CsCoCl_3 \cdot 2H_2O$ as a function of the magnetic field $\vec{H}$ parallel to the $\vec{a}$ direction at various temperatures; open circle—1.1 K, ×—4.2 K, open square—4.8 K, solid oval—10 K, open triangle—11.16 K, open oval—13.1 K, solid square 14.8 K, solid triangle—20.3 K, solid circle—77.3 K.

in which the transition to this "weak-ferromagnetic" state takes place broadens with increasing temperature and although the magnitude of σ_0 obtained by extrapolation does depend on the field from which one extrapolates, a measureable induced moment is observed up to 18 K on extrapolation from 20 kOe (Fig. 12).

In order to study the behavior of the spin system in an applied magnetic field at low temperatures, we performed rotation experiments in various fields at 1.1 K (Fig. 13). Although the principle of these experiments is similar to that of the NMR rotation experiments, the fact that we observe the magnetization directly allows us to obtain additional information about the magnetic states above and below the critical field. For $H > H_c$ the magnetization has a much larger maximum along $\vec{a}$ and the magnitude of σ varies approximately as $\cos\theta$ as we rotate H away from $\vec{a}$ toward $\vec{b}$ or $\vec{c}$. At a critical angle θ_c the magnetization decreases quite suddenly as we pass the phase boundary shown in Figs. 4 and 5.

The cosine behavior of σ near the $\vec{a}$ axis can only be understood if the anisotropy of the system is very large (thus providing another check on the Ising-like behavior).

TABLE III. Saturation magnetization and g values along the crystallographic axis as obtained from high-field measurements.

Crystal axis	Saturation magnetization (emu/g)	g factor
$\vec{a}$	31	3.8
$\vec{b}$	47	5.8
$\vec{c}$	53	6.5

B. Interpretation

We can explain, at least qualitatively, all of the observed magnetization results by the following set of assumptions: (i) the magnetic moment structure[11] deduced by NMR (Fig. 8); (ii) strong Ising interaction in the chains; (iii) weak isotropic exchange between the chains.

The Ising-like behavior is assumed to mean that a given moment has a fixed position in the crystallographic frame except for the possibility of reversing its direction. Consequently, application of a field greater than H_c in the $\vec{a}$ direction is sufficient to overcome the antiferromagnetic coupling between spins in adjacent ac planes, allowing all of the spins in alternate planes to reverse, thus reversing their net moments and inducing a "weak-ferromagnetic

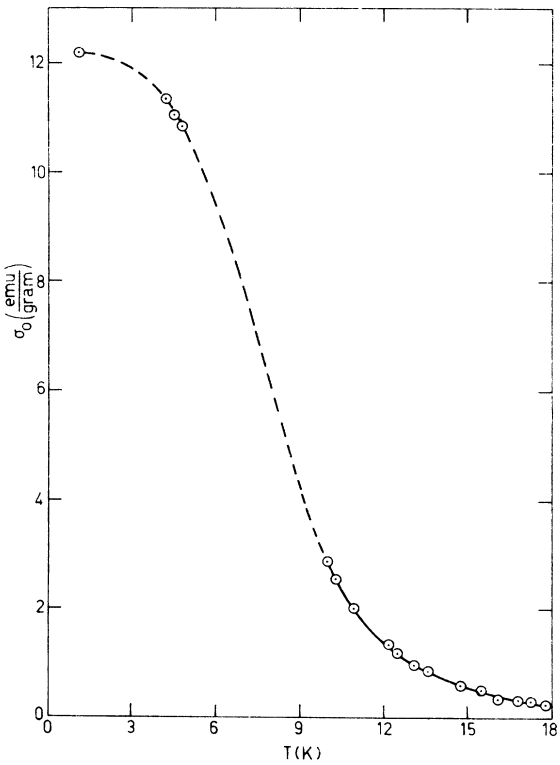

FIG. 12. Induced ferromagnetic moment $\vec{\sigma}_0$ (extrapolated from 20 kOe) as a function of temperature.

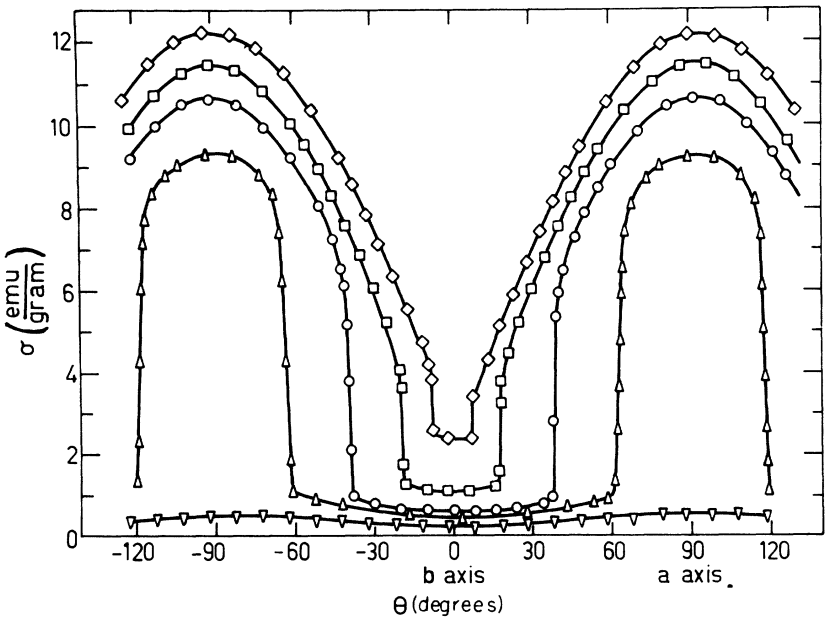

FIG. 13. Magnetization of $CsCoCl_3 \cdot 2H_2O$ in the *ab* plane as a function of the angle between the magnetic field and the $\vec{b}$ axis at a temperature $T = 1.1$ K; inverted triangle—2.3 kOe, triangle—3.2 kOe, circle—4.6 kOe, square—9 kOe, diamond—15 kOe.

moment" parallel to H.

Using the saturation-magnetization measured in high fields and the 10 emu/g discontinuity at the critical field, we obtain a canting angle of 10°, in excellent agreement with the NMR results.

The Ising nature explains the rotation diagrams, since neither the real moments nor their projections on the $\vec{a}$ axis are free to follow the field.

In order to understand both the non-Curie-Weiss behavior in the susceptibility above T_N and the induced moment above T_N, we invoke the fact that the Ising interaction is the dominant interaction, and is along the chains in the $\vec{a}$ direction. At temperatures well above T_N correlations between spins in the chain begin to be effective, giving rise to a correlation length which we can visualize as a short segment of a chain with a net moment in the $\vec{a}$ direction, antiferromagnetically aligned in $\vec{c}$ and having no component along $\vec{b}$. The application of a field tends to align the net moments producing an induced net moment in the $\vec{a}$ direction but no moment along either $\vec{b}$ or $\vec{c}$. The magnitude of this moment will increase with increasing correlation length and therefore with decreasing temperature until three-dimensional ordering due to interchain interactions takes place at T_N.

The susceptibility derived from the magnetization measurements will be larger than expected from the Curie-Weiss law in the $\vec{a}$ direction, will look more or less Curie-Weiss along $\vec{b}$, and have some intermediate behavior along $\vec{c}$. Silvera, Thornley, and Tinkham[12] have calculated the susceptibility of α-$CoSo_4$ which is also a canted four-sublattice system and predict a behavior similar to that which we observe in $CsCoCl_3 \cdot 2H_2O$.

VI. ANTIFERROMAGNETIC RESONANCE

A. Experimental Results

Antiferromagnetic resonance was performed at a variety of frequencies between 9 and 75 GHz at temperatures from 1 to 3.4 K and in fields up to 10 kOe. The sample was placed on the wall or end of a shorted X-band waveguide immersed in liquid helium. The X-band guide was coupled by various transitions to very simple reflection spectrometers in the ranges 9–12, 18–26, 34–35, and 65–76 GHz.

There are three features of interest in the experimental results: (i) The intensity of the resonance, which was zero at 3.4 K, went through a maximum at 1.8 K and decreased exponentially down to the lowest temperature available (Fig. 14). (ii) At low frequencies ($\nu < 25$ GHz) only one resonance was observed at $H = H_c = 2800$ Oe. The angle dependence of this resonance was the same as that of the critical fields observed in the NMR and magnetization measurements (Fig. 5). (iii) The frequency (ν) vs field (H) diagram (Fig. 15) gives an H_c of 2800 Oe and a ν_0 of 90 ± 10 GHz.

At higher frequencies the lines always appeared to double—a fact which we do not understand. No resonances were observed above 3.4 K at any frequency so that independent g values were not obtainable from paramagnetic resonance.

B. Interpretation

The temperature, angle, and frequency dependence of the AFMR can be explained only by assuming that we are observing spin-cluster resonance in an essentially Ising-like system[3,13,14] rather than the normal AFMR in a Heisenberg system. Although

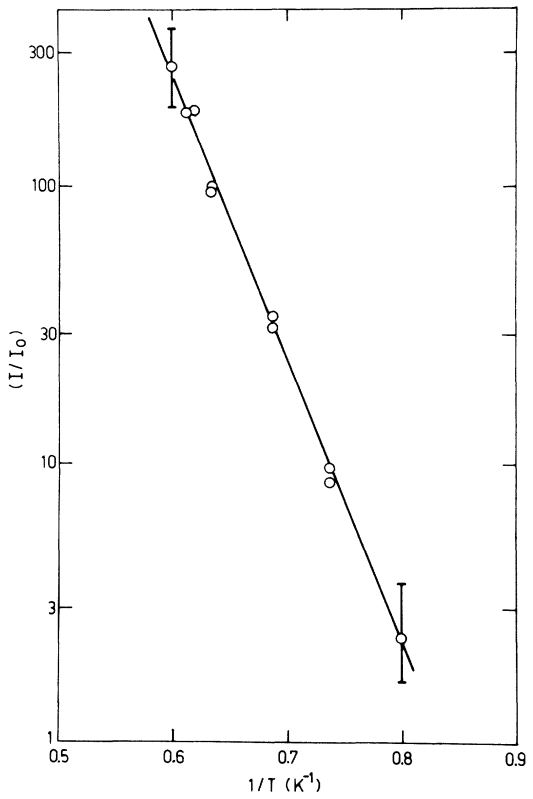

FIG. 14. Spin-cluster-resonance intensity as a function of reciprocal temperature.

we will develop a detailed model of the exchange interactions in Sec. VIII, a few general comments are appropriate here.

The concept of a spin cluster, as first suggested by Date and Motokawa,[13] involves the excitation of groups of spins in a strongly exchange-coupled Ising system. The energy of excitation of an n-fold cluster in an isolated—for example, ferromagnetically coupled—chain is given by

$$E_n = 4J^a S_z^2 + n(g\mu_B S_z H).$$

The exchange part of the excitation energy is independent of the size of the cluster, only the Zeeman energy depends on n. If J^a is large then we can see that excitation of a onefold cluster requires a large amount of energy and will be observable in the infrared. On the other hand, the transition $n=i$ to $n=i+\alpha$ for $i>0$ will involve only the Zeeman energy of α moments and will occur in the microwave region. These are what Date called spin-cluster resonances.[13] They are observable only when the $n=1$ clusters are thermally excited and therefore will have an intensity depending on the number of $n=1$ clusters which at low fields and low temperature depends on[13] $e^{E_i/kT}$, thus giving a measure of J^a.

The addition of interchain exchange interactions gives rise to a splitting of the previously degenerate E_n levels at $H=0$ and thus a ν_0 which is a measure of all the interchain couplings. If one of the interchain couplings is antiferromagnetic, the possibility exists for a metamagnetic transition at a critical field which is proportional to the antiferromagnetic exchange interaction. We expect that a detailed model of the spin system and the exchange interactions will allow us to interpret the temperature dependence of the intensity, the zero-field resonance frequency, and the critical field in terms of particular exchange constants.

VII. SUMMARY

The set of measurements which we have made has given us a model of the magnetic structure of $CsCoCl_3 \cdot 2H_2O$ which appears relatively complete and complex.

From specific heat we found that there is an anomaly at 3.38 K which (referring to other experimental results) can be attributed to three-dimensional ordering. The fact that only 16% of the theoretical entropy appears under the peak suggests very strongly that magnetic ordering in a lower dimension may appear at higher temperatures.

The NMR results give us a magnetic space group, and, with the additional calculation of the field at the proton site due to an array of dipoles, allow us to postulate a four-sublattice noncollinear antiferromagnetic spin array in which the magnetic

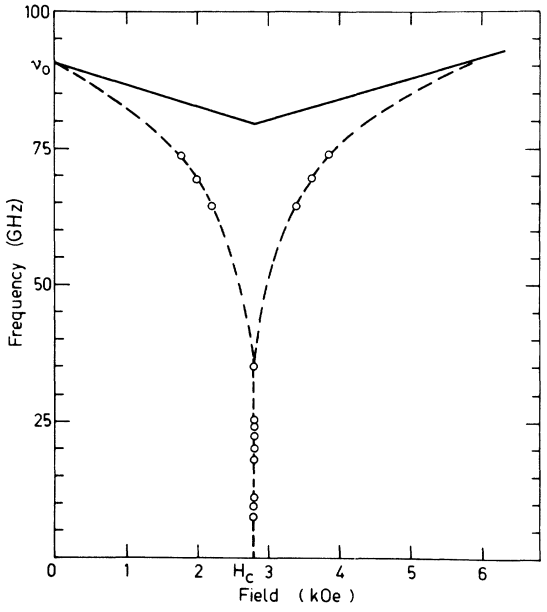

FIG. 15. Spin-cluster-resonance frequency as a function of applied field in the $\vec{a}$ direction. The dotted line is the best fit to the experimental points. The solid line is the theoretical curve normalized to H_c and ν_0.

moments are canted 10° from the $\vec{c}$ axis in the *ac* plane.

The magnetization data show a discontinuity at the critical field with an induced magnetic moment in the $\vec{a}$ direction which is 20% of the computed saturation value. This net moment could be observed up to 18 K as one would expect if correlations were important up to temperatures much higher than the three-dimensional ordering temperature.

The AFMR results confirm the Ising-like behavior. Combining these results with the postulated model one can compute the intrachain and the two interchain exchange interactions.

VIII. EXCHANGE PARAMETERS

In order to make a detailed calculation of the magnetic properties of the system we will write a Hamiltonian in the effective spin $=\frac{1}{2}$ variables having the following rather unusual form:

Dominant intrachain interaction; antiferromagnetic and Ising-like

$$-\sum_i J^a S_i^a S_{i+1}^a \ .$$

Intrachain canting; Dzyaloshinski-Moriya (D-M)

$$-\sum_i \vec{D}\cdot(\vec{S}_i \times \vec{S}_{i+1}) \ ,$$

where, for simplicity, $\vec{D}$ is assumed to be parallel to the $\vec{b}$ axis. The D-M term is allowed by symmetry and may be very large since $D \propto (g-2)/g$ which in our case can be 0.7.

Interchain interactions; isotropic

$$-\sum_i J^b \vec{S}_i \cdot \vec{S}_{i+1} \ ,$$

$$-\sum_i J^c \vec{S}_i \cdot \vec{S}_{i+1} \ .$$

Whether the interchain interactions are, in fact, isotropic cannot be determined from experiment since the possible anisotropies are masked by the large anisotropy in the dominant interaction. Since each spin has two nearest neighbors of each type, the factor of 2 is included in the exchange constants The resultant Hamiltonian is

$$\mathcal{H} = -J^a S_1^a S_2^a - \vec{D}\cdot(\vec{S}_1 \times \vec{S}_2) - J^b \vec{S}_1 \cdot \vec{S}_2 - J^c \vec{S}_1 \cdot \vec{S}_2, \tag{1}$$

where $\vec{S}_1$ and $\vec{S}_2$ are neighboring spins in the $\vec{a}$, $\vec{b}$, and $\vec{c}$ directions. In view of the experimental evidence reviewed in Secs. III and V, and the well-established linear chain behavior of the isomorphic $CsMnCl_3 \cdot 2H_2O$, we assume J^a to be larger than J^b and J^c. We can evaluate D in terms of J^a by noting that if in equilibrium the spins make an angle ϕ_s with the crystallographic $\vec{c}$ axis (Fig. 16),

$$E = -J^a S_1 \cos\phi_s S_2 \cos(\pi - \phi_s) - DS_1 S_2 \times \sin(\pi - 2\phi_s) + J^b S_1 S_2 - J^c S_1 S_2 \ . \tag{2}$$

Setting

$$\frac{\partial E}{\partial \phi_s} = 0 = -J^a S^2 \sin 2\phi_s - 2DS^2 \cos 2\phi_s \ ,$$

we obtain

$$\tan 2\phi_s = -2D/J^a \ . \tag{3}$$

Consequently, if we know ϕ_s we can evaluate D. In order to determine ϕ_s we must note that our experiments give us ϕ_m, the angle between the magnetic moment and the $\vec{c}$ axis. In order to obtain ϕ_s from ϕ_m we must make some assumptions about the principal axes of the g tensor.

We assume that the principal axes of g are determined by the local coordination axes and define $g_\perp$ to be parallel to the Cl_I-Co-Cl_I axis, $g_\parallel$ to be parallel to a line bisecting the angle formed by O-Co and Co-Cl_{II}, and g_b to be parallel to the $\vec{b}$ axis (Figs. 1 and 16). Using g_a and g_c from Table III and $\beta = 26°$ we compute $g_\parallel = 7.1$ and $g_\perp = 2.4$. Since $g_b = 5.8$ these values do not appear to satisfy the usual "rule of thumb" for Co^{2+} that the sum of the principal values equals 13.

We have concluded experimentally that $\phi_m = 10°$. Using $\vec{\mu} = \overleftrightarrow{g}\cdot\vec{S}$ we obtain $\phi_s = -14.5°$. Inserting this value in (3), we obtain

$$D = -0.28J^a .$$

At the same time using $g_\parallel$ and $g_\perp$ as given above, we

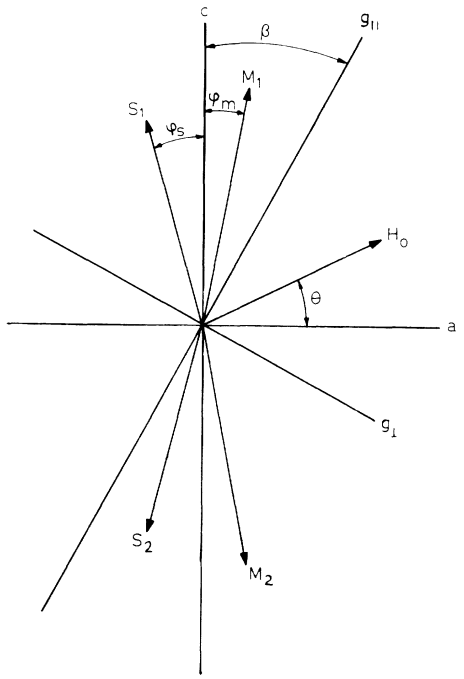

FIG. 16. Geometrical disposition of $\vec{M}$, $\vec{S}$, $\vec{H}$, and $\overleftrightarrow{g}$ tensor for one set of sublattices. The $\overleftrightarrow{g}$ tensor is that associated with $\vec{M}_1$ and $\vec{S}_1$.

compute $\mu = 2.8\mu_B$ for the equilibrium value of the magnetic moment.

In terms of the angles defined in Fig. 16, we have, for one spin at $T = 0$,

$$E_1 = J^a S^2 \cos^2\phi_s - DS^2 \sin 2\phi_s + J^b S^2 - J^c S^2 - \mu_B \vec{S} \cdot \overleftrightarrow{g} \cdot \vec{H}. \quad (4)$$

With H applied along $\vec{a}$ ($\theta = 0$) the Zeeman term becomes $-\mu_B S g_{\phi_m} H \sin\phi_m$, where g_{ϕ_m} is the g value in the equilibrium direction.

To obtain an expression for the critical field in the $\vec{a}$ direction, we equate the energies of the spin system before and after spin reversal. Recall that all the the spins in a given ac plane have their net moments along $+\vec{a}$, whereas those in the adjacent planes are along $-\vec{a}$. The total energy of all the spins is

$$E_{\mathrm{TOTAL}} = N(J^a S^2 \cos^2\phi_s - DS^2 \sin\phi_s + J^b S^2 - J^c S^2), \quad (5)$$

where the Zeeman terms due to adjacent planes cancel. After spin reversal

$$E_{\mathrm{TOTAL}} = N(J^a S^2 \cos^2\phi_s - DS^2 \sin 2\phi_s - J^b S^2 - J^c S^2 - \mu_B g_{\phi_m} SH \sin\phi_m), \quad (6)$$

where *only* the sign of the J^b term has changed because *only* nearest neighbors in the $\vec{b}$ direction have reversed.

Equating these two energies and solving for H_c we have

$$H_c(\theta = 0) = \tfrac{1}{2} \left| J^b \right| S/\mu_B g_{\phi_m} \sin\phi_m. \quad (7)$$

If H is along the $\vec{c}$ direction ($\theta = \frac{1}{2}\pi$) the same calculation gives

$$H_c(\theta = \tfrac{1}{2}\pi) = (|J^a| \cos^2\phi_s + |D| \sin 2\phi_s + |J^b|)S/\mu_B g_{\phi_m} \cos\phi_m \ . \quad (8)$$

In general, this is a much larger number than that of Eq. (7).

To compute the energy necessary to excite a spin cluster, we consider the change in energy of a given spin and its six nearest neighbors when the given spin is reversed. Calling $E(i)$ the energy of the system when an i-fold cluster is excited, we obtain, for $H < H_c$ and $\theta = 0$,

$$E(i) = -4S^2[J^a \cos^2\phi_s - D \sin 2\phi_s + i(J^b - J^c)] \pm 2i\mu_B S g_{\phi_m} H \sin\phi_m, \quad (9)$$

where the $\pm$ sign refers to clusters in adjacent ac planes with net moments in the opposite direction.

For the excitation of the onefold cluster we get

$$h\nu_1 = E(1) - E(0) = |J^a| \cos^2\phi_s + |D| \sin 2\phi_s + |J^b| + |J^c| \pm g_{\phi_m} \mu_B H \sin\phi_m \quad (10)$$

while, for the spin-cluster resonance,

$$h\nu = E(i+1) - E(i) = + |J^b| + |J^c| \pm g_{\phi_m} \mu_B H \sin\phi_m. \quad (11)$$

With $H > H_c$ the net moments all lie in the same direction so that we now have

$$E(i) = -4S^2[J^a \cos^2\phi_s - D \sin 2\phi_s - i(J^b + J^c)] + 2i\mu_B g_{\phi_m} SH \sin\phi_m \quad (12)$$

and again, for the onefold cluster,

$$h\nu_1 = E(1) - E(0) = + |J^a| \cos^2\phi_s + |D| \sin 2\phi_s + |J^b| + |J^c| + g_{\phi_m} \mu_B H \sin\phi_m \quad (13)$$

and, for the spin-cluster resonance,

$$h\nu = E(i+1) - E(i) = |J^b| + |J^c| + g_{\phi_m} \mu_B H \sin\phi_m. \quad (14)$$

The onefold excitation occurs in the infrared because of the large intrachain exchange but the spin-cluster resonance occurs in the microwave range with a zero-field resonance

$$h\nu_0 = + |J^b| + |J^c| \ . \quad (15)$$

The theoretical curves are plotted as solid lines in Fig. 15 normalized to the experimental H_c and ν_0. It is clear that there is a serious discrepancy in that the experimental data goes to zero frequency at H_c, whereas the theoretical curves remain at large ν. Torrence and Tinkham[14] have shown that the addition of non-Ising terms to the Hamiltonian introduces terms in the energy which are not linear in the field and which therefore agree better with the experimental curves. We will not apply these terms to our system but rather assume that neither H_c nor ν_0 are seriously modified by their inclusion and evaluate the exchange parameters using (7) and (15).

The intensity of the spin-cluster resonance is exponential in $E(1) - E(0)$ as predicted by Eq. (10). Experimentally we have $I \approx e^{-20/T}$, $H_c = 2800$ Oe, $\nu_0 = 90 \pm 10$ GHz, $\phi_m = 10°$, and $g_{\phi_m} = 5.6$. Using these values we obtain

$$J^a = -12.7 \text{ K}, \quad J^b = -0.2 \text{ K}, \quad J^c = +4.5 \text{ K}, \quad D = +3.6 \text{ K}.$$

The J^a defined in (1) is only part of the intrachain energy. The total intrachain excitation energy, including D, is 15 K.

IX. DISCUSSION

In Table IV we have tabulated the details of the model and indicated the measurements which are responsible for arriving at each of the results.

TABLE IV. Summary of measurements and the inferred magnetic structure of $CsCoCl_3 \cdot 2H_2O$.

	Specific heat	NMR	Magnetization susceptibility	AFMR
T_c	3.38	3.38	3.4	...
Behavior for $T < T_c$		Antiferromagnetic	Antiferromagnetic	Antiferromagnetic
Behavior for $T > T_c$	Large amount of entropy	Paramagnetic	Induced moment	...
H_c (kOe)	...	2.85	2.9	2.8
$H_c(\theta)$	...	$\cos\theta$	$\cos\theta$	$\cos\theta$
Ising like?	...	Probably	Yes	Yes
Magnetic space group	...	$P_{2b}cca'$	...	$P_{2b}cca'$
Canting angle	...	10°	10°	0°
Intrachain exchange (K)	Probably large	<0	Probably large	-16
Interchain J^b	...	-0.2	-0.2	-0.2
exchange J^c (K)	...	>0		$+4.5$

Preliminary neutron-diffraction results[15] confirm the space group to be $P_{2b}caa'$ and the magnitudes of the magnetic moments along $\vec{a}$ and $\vec{c}$. Although we believe the model outlined above gives a correct qualitative description of the magnetic behavior there are some discrepancies:

(i) The most serious discrepancy appears in the evaluation of the intrachain exchange which is given as 16 K by the temperature dependence of the intensity of the spin-cluster resonance and ~70 K by the admittedly rather unsatisfactory analysis of the specific-heat data. Although the theory of the resonance intensity seems rather simple and straightforward,[13] the only other case for which measurements have been made, those by Date on $CoCl_2 \cdot 2H_2O$, seem to suffer from the same malaise.

Date does not explicitly compare the values obtained from the temperature dependence of the spin-cluster resonance[16] with the values obtained by Narath[17] for the exchange interactions, $J_0 = 9.3$ K; $J_1 = -4.4$ K; $J_2 = -1$ K. Since the excitation of a single spin involves doing work against all of the exchange interactions, the intensity should behave like $e^{15/T}$. If one scales crudely from Fig. 10 of Ref. 16 one obtains approximately $e^{3/T}$. This is a factor of 5 smaller than the theoretical value, which, for whatever it is worth, is similar to our result.

(ii) The calculation of the remaining exchange parameters is based on the strongly Ising-like behavior of the system. Additional small transverse components of the exchange interaction cause a shift in the energy levels of the clusters downwards.[14] This shift is most pronounced near H_c and will affect the calculated values of the exchange parameters.

(iii) There are three values which we have available for the equilibrium magnetic moment: $\mu = 2.8\mu_B$ obtained from the magnetization measurements, $\mu = 2.25\mu_B$ which gave the best results when used in the dipole calculation (Sec. IV) and a preliminary neutron-diffraction result $\mu = 2.6\mu_B$.[15] Although there is a rather large amount of scatter in these values, their dependence on such unknown factors as the orientation of the g tensor, contact hyperfine interactions, etc., indicates that a mean value of $\mu = (2.5 \pm 0.3)\ \mu_B$ is not so unreasonable.

(iv) Susceptibility measurements[1] in the isomorphic $CsMnCl_3 \cdot 2H_2O$ showed a broad maximum above T_N which could be attributed to the spin correlations within the chains. That such an effect is not observed in our case can be understood qualitatively by treating the linear chain of spins as the sum of an antiferromagnetic and a ferromagnetic chain with appropriate moments. Referring to calculations by Katsura,[18] it is seen that the exponential contribution of the ferromagnetic component of the chains to the susceptibility can easily obscure any broad maximum due to the antiferromagnetic coupling in the chains. In $CsMnCl_3 \cdot 2H_2O$ the coupling in the chains was purely antiferromagnetic and no ferromagnetic contribution appears.

In summary, the application of a simple and probably not strictly correct Hamiltonian to the results of a large number of essentially macroscopic measurements has resulted in the analysis of a complex magnetic system. Answers to the remaining questions await both a better theoretical approach and the detailed results of the neutron-scattering ex-

periments.

ACKNOWLEDGMENTS

We are much indebted to Professor A. R. Miedema and Dr. F. A. Muller for the use of the high-field magnet in the "Natuurkundig Laboratorium" of the University of Amsterdam and to Dr. Y. Tamminga who assisted with these measurements. We want to acknowledge several valuable discussions with Professor P. van der Leeden and Dr. L. G. Polgar. Thanks are due to C. W. Spoor and J. A. M. Verbruggen who assisted with the magnetization measurements at Eindhoven University of Technology.

---

*Some of this work was performed as part of the research program of the "Stichting voor Fundamenteel Onderzoek der Materie" (FOM) with financial support of the "Nederlandse Organisatie voor Zuiver-Wetenschappelijk Onderzoek" (ZWO). A. C. Botterman is a collaborator of FOM.

†Present address: Department of Physics, Michigan State University, East Lansing, Mich.

[1]T. Smith and S. A. Friedberg, Phys. Rev. 176, 600 (1968).

[2]J. Skalyo, G. Shirane, S. A. Friedberg, and H. Kobayashi, Phys. Rev. B 2, 1310 (1970).

[3]J. B. Torrance, Jr. and M. Tinkham, Phys. Rev. 187, 595 (1969).

[4]W. J. M. de Jonge, K. V. S. Rama Rao, C. H. W. Swüste, and A. C. Botterman, Physica 51, 620 (1971).

[5]N. Thorup and H. Soling, Acta Chem. Scand. 23, 2933 (1969).

[6]The calibration was performed against a similar germanium thermometer for which the calibration had been supplied by the manufacturer: CryoCal, Inc., Riviera Beach, Fla.

[7]C. Domb, Advan. Phys. 9, 149 (1960).

[8]R. D. Spence and P. A. van Dalen, Acta Cryst. A24, 494 (1968).

[9]W. Opechowski and R. Guccione, *Magnetism*, edited by G. T. Rado and H. Suhl (Academic, New York, 1965), Vol. 2A, Chap. 3.

[10]J. Wiebes, W. S. Hulscher, and H. C. Kramers, Appl. Sci. Res. 11B, 213 (1965).

[11]Although one would normally describe this as a spin structure, the very anisotropic g tensor indicates that the spins and magnetic moments point in quite different directions. The NMR measurements give us the direction of the sublattice magnetization and hence the magnetic moments.

[12]I. F. Silvera, J. H. M. Thornley, and M. Tinkham, Phys. Rev. 136, A695 (1964).

[13]M. Date and M. Motokawa, Phys. Rev. Letters 16, 1111 (1966).

[14]J. B. Torrance and M. Tinkham, Phys. Rev. 187, 587 (1969).

[15]B. van Laar and A. L. M. Bongaarts (private communication).

[16]M. Date and M. Motokawa, J. Phys. Soc. Japan 24, 41 (1968).

[17]A. Narath, J. Phys. Soc. Japan 19, 2245 (1964).

[18]S. Katsura, Phys. Rev. 127, 1508 (1962).